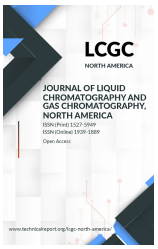

Journal of Liquid Chromatography and Gas Chromatography, North America
https://technicalreport.org/lcgcnam

LC GC N. Am., Vol. 44, No.1, 20-25, 2026

Technical Reports Press

RESEARCH ARTICLE

Kinetic–Capacitive–Durability Coupling in ZIF-67-Derived Ni Single-Atom/Co–N–C Electrocatalysts for Water Splitting

Benjamin Scott[1*]

[1]*Institute for Environmental Analysis Greenfield University United States*
[*]*Corresponding author*

Corresponding author:
banjamin_chemist@gmail.com

Received: 20 October 2025
Accepted: 21 February 2026
Available online: 30 March 2026

Abstract

An effective non-noble-metal electrocatalyst for alkaline water electrolysis must enable fast electron transfer, high reactivity at the surface-liquid interface, stable active-site chemistry, and minimal current leakage upon prolonged bias application. Alkaline hydrogen evolution catalysts based on Co–N–C materials derived from ZIF-67 precursors are appropriate choices in this regard owing to the ability of their cobalt-imidazolate chemistry to tune metal centers, nitrogen incorporation, and conductive porosity of the carbon matrix simultaneously. In this work, we analyze the electrochemical properties of a series of sequentially chemically linked ZIF-67 (unchanged), ZIF-67@DCD (dicyandiamide), and NiSAs@ACNTF (nickel addition) catalysts. Combination of LSV, CV, and CA analyses allows for differentiation between real improvements of catalytic kinetics and alterations of double-layer capacitative properties. The latter show a decreasing trend in the CV-based sequence: ZIF-67 ($7.28\,\mathrm{mF\,cm^{-2}}$) > ZIF-67@DCD ($5.14\,\mathrm{mF\,cm^{-2}}$) > NiSAs@ACNTF ($4.89\,\mathrm{mF\,cm^{-2}}$). However, the LSV profile selects NiSAs@ACNTF as the best-performing candidate. Thus, higher catalytic activity of the catalyst with nickel addition cannot be accounted for by the growth of its capacitive interface, and should rather be attributed to better active site chemistry and increased electronic interaction within the nitrogen-doped carbon host. CA data reveal the stability of the activity edge during a ten-hour operating regime after the initial activation process. The key finding of the work lies in a combined analysis of kinetic, capacitive, and durability parameters that characterize accessible surface, catalytic performance, kinetic rate, and retention within a precursor family.

Keywords: ZIF-67; non-noble-metal electrocatalyst; water splitting; nickel single atoms; cyclic voltammetry; double-layer capacitance; chronoamperometry; catalyst durability

1. Introduction

Electrochemical water splitting offers a straightforward means of turning electrical energy derived from renewables into stored chemical fuel in the form of hydrogen. The efficiency of such an energy transformation is dictated by the kinetic properties of hydrogen evolution reaction (HER) and oxygen evolution reaction (OER), both requiring highly efficient catalysts able to work at very low overpotential and remain active upon long-term application of strong potential bias. Currently, Pt-based compounds retain excellent performance for HER, whereas IrO_2 or RuO_2 are typical catalysts for OER; however, the use of noble metals presents severe restrictions on wide-scale application. This constraint has led to extensive research into earth-abundant electrocatalysts composed of Ni, Co, Fe, nitrogen-doped carbon, metal sulfides/phosphides/nitrides/oxides, and hybrid carbon matrices [1–5].

One class of precursors suitable for fabrication of catalytically active materials is metal-organic frameworks (MOFs). Ordered structures involving ligands coordinated with a metal center allow the creation of carbon nanomaterials characterized by flexible chemical composition and structural configuration of metal, nitrogen, and carbon moieties. ZIF-67, being a representative of imidazole MOFs containing cobalt ions, is extensively studied due to its capacity to create various combinations of cobalt, nitrogen, and carbon in the form of Co–N–C units, cobalt nanoparticles, and doped carbon [6, 7]. In addition, the use of di-

Cite as: Naveed Ahmad (2026). Kinetic–Capacitive–Durability Coupling in ZIF-67-Derived Ni Single-Atom/Co–N–C Electrocatalysts for Water Splitting. LC GC N. Am., 44(1) (2026) 20-25.

cyandiamide (DCD) as a co-solvent facilitates nitrogen chemistry and carbon modification, and nickel introduction into the catalyst leads to additional active sites as well as alteration of electronic configuration [6, 7]. The variety of chemical aspects makes ZIF-67 derivatives attractive in separation of individual precursor contributions, generation of active sites, and charge transport mechanisms.

One of the challenges associated with electrocatalyst characterization stems from a misconception about geometric current. The higher current delivered by a given material cannot be directly correlated to either a higher surface area, presence of intrinsically more active reaction sites, more efficient charge transfer, or higher catalytic durability. The values of onset potential, overpotential at a fixed current density, Tafel slope, double-layer capacitance, scan rate dependence, and chronoamperometric measurements provide distinct data related to different physical parameters and cannot be considered equivalent. Proper characterization of an electrocatalyst requires consistent electrode preparation, reporting electrolyte and reference electrode type, consideration of internal resistance contribution, precise measurement of mass loading, Faradaic efficiency evaluation, and stability assessment beyond mere visual analysis of polarization curves [8–10].

In this study, we ask whether the superior response of nickel-doped NiSAs@ACNTF is related to an increased electrochemically accessible area or improved kinetics and durability. The distinction between these two cases is crucial because increased charge accumulation on a highly capacitive material does not imply that all reaction sites are optimally active. At the same time, materials showing lower double layer capacity might demonstrate higher activity if their sites are better designed in terms of energetics and conductivity. Moreover, enhanced stability is also critical in the context of water splitting electrocatalysis. This paper makes three independent contributions. First, it evaluates the differences among ZIF-67, ZIF-67@DCD, and NiSAs@ACNTF using the same characteristic set. Second, it detects the clear reversal between capacitance and activity measured in CV and LSV modes, respectively, thus revealing the dissociation between apparent accessibility and productivity of a Ni-containing catalyst. Third, it interprets the electrochemical results in light of chemical transformations that include reconfiguration of N/C matrix in the case of DCD and introduction of Ni into the catalytically active structure.

2. Materials and Electrochemical Analysis

2.1. Catalyst series and measurement conditions

The catalyst sequence contains three ZIF-67-derived materials. The first material, ZIF-67, is obtained from pristine ZIF-67. The second material, ZIF-67@DCD, introduces DCD into the ZIF-67 precursor to modify the nitrogen/carbon environment before thermal conversion. The third material, NiSAs@ACNTF, incorporates nickel into the ZIF-67@DCD precursor, yielding a Ni-containing MOF-derived electrocatalyst. The precursors are pyrolyzed under argon at 750 °C, producing carbonized catalysts for electrochemical testing [7].

Catalyst inks are prepared by dispersing catalyst powder in a water/isopropanol/Nafion mixture. The working electrode is produced by drop-casting the ink onto carbon cloth at a mass loading of $0.3\,\mathrm{mg\,cm^{-2}}$. A Hg/HgO electrode serves as the reference electrode and a graphite rod serves as the counter electrode. Potentials are reported on the reversible hydrogen electrode (RHE) scale after reference conversion according to

$$E_{\mathrm{RHE}} = E_{\mathrm{Hg/HgO}} + E^{0}_{\mathrm{Hg/HgO}} + 0.059\,\mathrm{pH}, \tag{1}$$

where 0.059 V is the Nernst slope at 25 °C. The electrochemical record includes LSV, scan-rate-dependent CV, and chronoamperometry for current-retention evaluation [7].

The comparison is internally controlled because the three catalysts share the same precursor family, electrode substrate, catalyst loading, and measurement configuration. Absolute comparison with external catalyst systems requires matched electrolyte composition, reference calibration, electrode area, catalyst loading, gas-product quantification, and resistance-correction conditions [9, 10]. The present analysis therefore emphasizes within-series ranking and descriptor coupling.

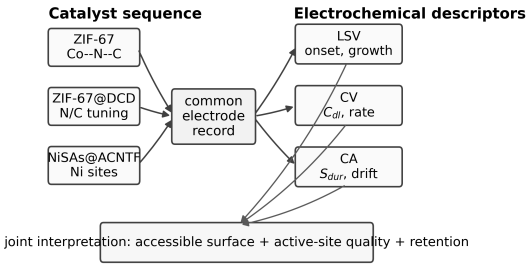

Figure 1: Coupled electrochemical evaluation of the ZIF-67-derived catalyst sequence. The same electrode record is interpreted through LSV, CV, and chronoamperometry to separate kinetic response, capacitive accessibility, and current retention within a common precursor family.

2.2. LSV-derived kinetic descriptors

The LSV response is expressed as $j(E)$, where j denotes geometric current density. For catalyst c, the onset descriptor is defined by a fixed current-density threshold,

$$E_{\mathrm{onset}}(c) = E\left(|j_c(E)| = j_{\mathrm{th}}\right), \tag{2}$$

where j_{th} is selected before fitting. A common threshold is essential because changing j_{th} can alter apparent onset values without changing the underlying polarization curve.

The Tafel slope is estimated from the kinetic region of

$$\eta = a + b\log_{10}|j|, \tag{3}$$

where η is the overpotential, a is the intercept, and b is the Tafel slope. The fitting interval excludes points dominated by capacitive current, mass-transport limitation, and near-zero-current noise. The local post-onset growth rate is further evaluated as

$$G(E) = \frac{\mathrm{d}|j(E)|}{\mathrm{d}|E|}, \tag{4}$$

so that the steepness of catalytic amplification can be compared across the catalyst sequence. A larger $G(E)$ after onset indicates that a smaller additional driving force produces a larger current response.

2.3. CV-derived capacitance and rate descriptors

The apparent double-layer capacitance is obtained from the scan-rate dependence of current in a potential region where non-Faradaic charging is dominant. At the selected potential, the anodic–cathodic current difference is

$$\Delta j = j_{\mathrm{a}} - j_{\mathrm{c}}, \tag{5}$$

with

$$\frac{\Delta j}{2} = C_{\mathrm{dl}}\nu, \tag{6}$$

where ν is the scan rate. The slope of $\Delta j/2$ against ν gives C_{dl}. When the plotted convention uses Δj rather than $\Delta j/2$, the slope must be divided by two before comparing catalysts. This distinction is necessary because an inconsistent convention changes the numerical value while preserving the qualitative trend.

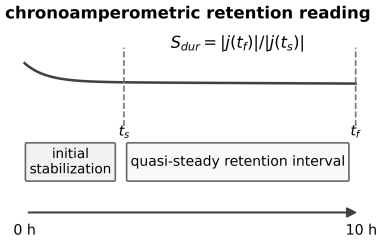

Figure 2: Chronoamperometric retention descriptor. The quasi-steady interval begins after the initial stabilization period, and current retention is evaluated from $|j(t_f)|/|j(t_s)|$ over the ten-hour operating window.

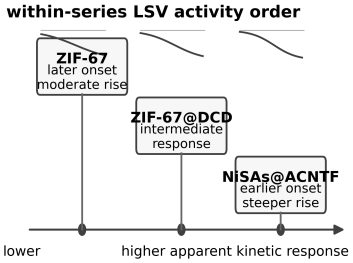

Figure 3: Within-series LSV activity order for the ZIF-67-derived catalysts. The Ni-containing material shows the earliest apparent onset and strongest post-onset response, whereas pristine ZIF-67 gives a weaker kinetic response despite having the largest capacitance.

Rate tolerance is assessed from the variation of a scan-rate-dependent descriptor $Q_c(v)$:

$$R_{\text{scan}}(c) = 1 - \frac{\sigma\left(Q_c(v)\right)}{\overline{Q_c(v)}}, \tag{7}$$

where σ is the standard deviation across tested scan rates and $\overline{Q_c(v)}$ is the corresponding mean. A higher R_{scan} indicates a more stable response across scan rates. When full CV traces are available, the relation

$$i(V) = a(V)v^{b(V)} \tag{8}$$

can distinguish diffusion-influenced behavior ($b \approx 0.5$) from surface-controlled capacitive behavior ($b \approx 1$). The current can also be partitioned as

$$i(V) = k_1(V)v + k_2(V)v^{1/2}, \tag{9}$$

where $k_1 v$ represents the surface-controlled contribution and $k_2 v^{1/2}$ represents the diffusion-influenced contribution [11–13].

2.4. Chronoamperometric stability descriptors

The chronoamperometric response $j(t)$ is evaluated after the initial wetting and equilibration interval. Current retention is defined as

$$S_{\text{dur}} = \frac{|j(t_f)|}{|j(t_s)|}, \tag{10}$$

where t_s is the start of the quasi-steady region and t_f is the final measurement time. Time-dependent drift is quantified using

$$j(t) = j_0 + \alpha t \tag{11}$$

for a linear drift model, and

$$j(t) = j_\infty + A\exp(-t/\tau) \tag{12}$$

for a relaxation model. Model selection is based on residual structure and adjusted goodness of fit. Reporting both S_{dur} and α prevents stability from being inferred only from the visual flatness of a current–time curve.

2.5. Coupled performance index

A normalized catalyst descriptor vector is defined as

$$\mathbf{P}_c = (A_c, K_c, C_c, R_c, S_c), \tag{13}$$

where A_c denotes apparent activity, K_c denotes kinetic favorability, C_c denotes capacitive accessibility, R_c denotes scan-rate robustness, and S_c denotes current retention. Each component is scaled from 0 to 1 within the catalyst set. For descriptors where smaller values are favorable, such as overpotential or Tafel slope, min–max scaling is inverted:

$$X_c^* = \frac{X_{\max} - X_c}{X_{\max} - X_{\min}}. \tag{14}$$

The combined index is

$$I_c = w_A A_c + w_K K_c + w_C C_c + w_R R_c + w_S S_c, \tag{15}$$

where the weights satisfy $\sum_i w_i = 1$. The index is a consistency check across descriptors; individual electrochemical quantities remain the primary evidence. Sensitivity to the weights should be examined when catalyst selection prioritizes activity, durability, cost, or rate response differently.

3. Results

3.1. LSV response identifies a kinetic gain after Ni incorporation

The comparative LSV response ranks NiSAs@ACNTF as the most active catalyst in the sequence. It reaches the cathodic current threshold at a less negative apparent potential than ZIF-67 and ZIF-67@DCD, and its post-onset current rises more sharply with applied potential. These features indicate a lower apparent kinetic barrier and stronger catalytic amplification after reaction initiation. Because the catalysts are evaluated with the same electrode preparation and electrochemical configuration, the relative order within the sequence is meaningful even when absolute current values are not used for external comparison.

The LSV order is mechanistically significant because it does not follow the capacitance order. If the activity increase were caused mainly by a larger electrochemically accessible area, the material with the largest CV-derived capacitance would be expected to give the strongest LSV response. The opposite relation is observed: pristine ZIF-67 has the largest apparent capacitance, while Ni-containing NiSAs@ACNTF shows the strongest catalytic response. The result indicates that nickel incorporation improves the productivity of active sites or charge-transfer pathways rather than merely expanding the capacitive interface.

3.2. CV-derived capacitance separates accessibility from catalytic activity

The scan-rate-dependent CV response gives a clear capacitance sequence. The apparent double-layer capacitance values are $7.28\,\text{mF}\,\text{cm}^{-2}$ for ZIF-67, $5.14\,\text{mF}\,\text{cm}^{-2}$ for ZIF-67@DCD, and $4.89\,\text{mF}\,\text{cm}^{-2}$ for NiSAs@ACNTF. These values are summarized in Table 1 and visualized in Figure 4. DCD modification and Ni incorporation therefore do not increase apparent capacitive area; instead, catalytic performance improves while capacitance decreases.

Table 1: CV-derived apparent double-layer capacitance for the ZIF-67-derived catalyst series.

Catalyst	Design variable	C_{dl} (mF cm^{-2})	Interpretation
ZIF-67	Pristine ZIF-67-derived carbon	7.28	Largest capacitive accessibility within the series.
ZIF-67@DCD	DCD-modified precursor	5.14	Lower capacitance with altered N/C interfacial structure.
NiSAs@ACNTF	Ni-incorporated ZIF-67@DCD	4.89	Highest LSV activity despite the smallest capacitance value.

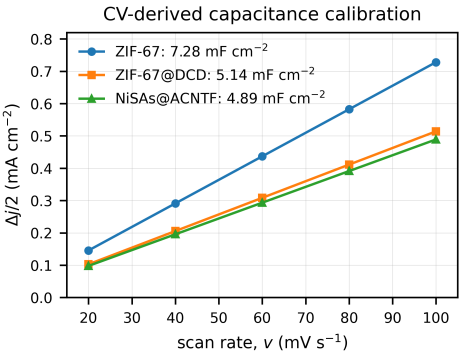

Figure 4: CV-derived capacitance calibration calculated from the reported C_{dl} values using $\Delta j/2 = C_{dl}v$. The slope order is ZIF-67 > ZIF-67@DCD > NiSAs@ACNTF, which is opposite to the LSV activity order.

This capacitance–activity separation is the central electrochemical observation. In porous carbon electrocatalysts, C_{dl} is often used as a proxy for wettable interfacial area, yet a large C_{dl} does not prove that the exposed surface contains kinetically optimal reaction centers. ZIF-67 provides the strongest capacitive response, whereas NiSAs@ACNTF provides the strongest catalytic response. The Ni-containing material therefore improves the catalytic value of the accessible interface, most plausibly through Ni-related coordination environments and stronger electronic coupling to the conductive scaffold.

3.3. Sequential precursor modification distinguishes N/C restructuring from Ni-site activation

The ZIF-67 → ZIF-67@DCD transition isolates the effect of DCD addition. DCD supplies nitrogen-rich decomposition products during pyrolysis and can alter the carbonization pathway, leading to a different N/C environment. The decrease in apparent capacitance from 7.28 mF cm^{-2} to 5.14 mF cm^{-2} shows that this modification does not simply create more interfacial charge-storage area. The more likely effect is redistribution of nitrogen coordination and carbon connectivity, with partial removal of less productive capacitive contributions.

The ZIF-67@DCD → NiSAs@ACNTF transition isolates the effect of nickel incorporation. The capacitance decreases only slightly, from 5.14 mF cm^{-2} to 4.89 mF cm^{-2}, while the LSV response improves markedly. This pattern supports a kinetic role for Ni-containing active sites rather than an area-expansion role. In Co–N–C/CNT-like environments, Ni can contribute through Ni–N coordination, Ni–Co electronic interactions, or CoNi-associated motifs embedded in N-doped carbon [6, 14, 15]. The electrochemical evidence does not assign a single atomic structure, but it strongly identifies active-site chemistry as the dominant source of performance improvement.

3.4. Chronoamperometry confirms short-term current retention

The chronoamperometric response of NiSAs@ACNTF remains nearly constant over the ten-hour test after the initial stabilization interval. This behavior shows that the high activity is not limited to a transient surface state that rapidly deactivates under constant potential. For water-splitting catalysts, this distinction is essential because high-surface-area materials can exhibit attractive initial currents and then lose activity through surface reconstruction, catalyst detachment,

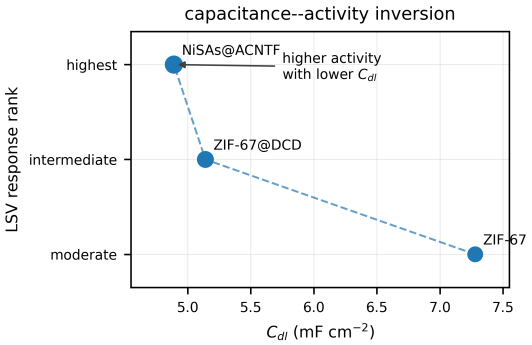

Figure 5: Capacitance–activity inversion in the catalyst series. The x-axis uses the measured C_{dl} values, while the y-axis gives the within-series LSV response rank; the Ni-containing catalyst combines the lowest capacitance with the strongest apparent activity.

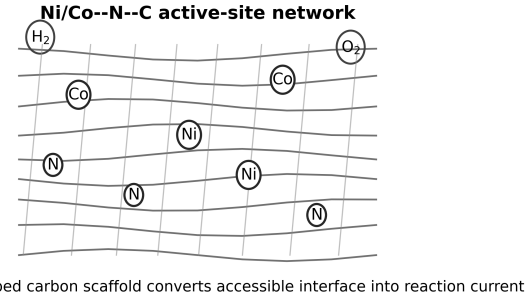

Figure 6: Site-level interpretation of the Ni/Co–N–C catalyst environment. Nickel- and cobalt-coordinated centers embedded in a conductive N-doped carbon scaffold can convert a smaller apparent capacitive interface into higher reaction current.

oxidation-state changes, blockage of active sites, or carbon corrosion. The ten-hour test supports laboratory-scale stability but does not establish electrolyzer-level durability. Practical operation requires higher current densities, longer run times, gas-product quantification, accelerated stress testing, and post-test structural characterization. The defensible conclusion is that NiSAs@ACNTF retains its activity during the tested operating window and is therefore the strongest candidate in this sequence for extended durability assessment under more demanding conditions. This interpretation aligns the validation with accepted electrocatalyst-testing expectations [9, 10].

3.5. Coupled descriptor assessment

Table 2 combines the LSV, CV, and chronoamperometric evidence. No single descriptor gives a complete assessment. ZIF-67 is favorable in capacitance but not in catalytic activity. ZIF-67@DCD occupies an intermediate state, indicating that DCD alters the electrochemical interface without generating the highest-activity configuration. NiSAs@ACNTF is strongest in apparent kinetic activity and current retention even though its capacitance value is the lowest. This combination provides direct evidence that activity and capacitive accessibility are decoupled in the Ni-containing material.

The combined descriptor assessment clarifies the design direction. Increasing porosity or capacitance alone is unlikely to deliver the best water-splitting performance. Synthetic optimization should target active-site electronic structure, interfacial conductivity, and structural retention under polarization at the same time. A minimum validation set for future ZIF-67-derived catalysts should include activity thresholds, Tafel behavior, C_{dl}, scan-rate response, electrochemical impedance, Faradaic efficiency, and extended chronoamperometric or chronopotentiometric testing.

Table 2: Combined electrochemical interpretation of the catalyst series.

Catalyst	LSV activity	C_{dl} value	Stability evidence	Interpretation
ZIF-67	Moderate	Highest	Not dominant in the retention comparison	Large capacitive interface does not produce the strongest catalytic response.
ZIF-67@DCD	Intermediate	Intermediate	Not dominant in the retention comparison	DCD modifies the N/C interface but does not maximize kinetic activity.
NiSAs@ACNTF	Highest	Lowest	Stable ten-hour response	Ni-containing sites improve apparent kinetics while retaining current output.

4. Discussion

4.1. Relevance of the kinetic-capacitive inversion

The key experimental finding here is the inversion between capacitance and electrocatalytic activity. ZIF-67 possesses the largest apparent capacitance, but NiSAs@ACNTF yields the highest current density in LSV analysis. This contradicts the expectation that increased electrochemically accessible area will yield improved water splitting performance. Current density is determined by the number of active sites, the intrinsic turnover capabilities of these sites, the electronic conductivity of the adjacent carbon matrix, and the catalytic stability in the operation period.

Nickel-based catalysts are especially good at enhancing these characteristics, even as they increase capacitance less efficiently. The presence of nickel can modify the adsorption energetics, enable new Ni–N or Ni–Co coordination complexes, and shift the electronic structure of the adjacent Co/N/C sites. The conductive structure provided by the nitrogen-doped carbon skeleton will ensure that this enhanced active surface performs well. Thus, a more modest capacitive interface can perform better due to increased kinetic capabilities of the active surface.

4.2. Implications of the study for MOF-derived catalyst development

For MOF-derived catalysts, modification of the catalyst precursor often results in changes to multiple material properties simultaneously. Morphology, pore wetting, metal speciation, nitrogen coordination, graphitization degree, and electronic conductivity can change together. If only the final current values obtained in LSV are analyzed, such complexity will hide which of these modifications was crucial to catalytic improvement. This study has identified two different modifying factors, both acting on different material properties.

This suggests that future research should focus not on maximizing the capacitance of the modified MOF catalyst, but on optimizing other aspects of its catalytic performance. High C_{dl} can be a useful feature of catalyst materials, but it is a supporting parameter in water splitting. The most efficient catalysts are those where other aspects of material properties have been optimized alongside the accessible area.

4.3. Verification of the conclusion via additional characterizations

The current experimental evidence provides strong verification of the conclusion since it relies on the chemically related sequence of catalyst materials, common electrode geometry and mass loading of electrodes, and multiple electroanalytic methods used. Since the LSV order of performance and current retention order are identical, while the order of C_{dl} is the inverse, kinetic–capacitive dissociation is quite solid for this particular catalyst sequence. In addition, the statement avoids claiming superiority against noble metal catalysts, which would need a direct comparison under similar conditions.

Further experiments should include high-current electrolysis in the application timeframe, rapid potential/current cycling, electrochemical impedance spectroscopy before and after the experiment, faradaic efficiency estimation based on gas collection, and analysis of the structure of the tested material after the experiment. Annular dark field scanning transmission electron microscopy can confirm the isolation of the metal atoms. X-ray absorption spectroscopy can analyze the coordination environments. X-ray photoelectron spectroscopy can determine the oxidation state of the surface. Raman spectroscopy can measure carbon disorder. And finally, density functional theory can analyze the energy of Ni–N, Co–N, and CoNi/N–C coordination motifs [1, 6]. All of these will provide a clear identification of the atomistic origin of the functional trend confirmed by the present results.

4.4. Boundaries of the conclusions

The conclusion made is most reliable in relative comparisons within the studied ZIF-67-derived catalyst series. Several limitations exist regarding general applicability of the statements made. First, C_{dl} is not an exact measurement of the number of active sites or the accessible area. Various aspects can affect it [11, 12]. Second, ten hours of chronoamperometry confirms only short-term laboratory stability, not long-term electrolyzer performance. Finally, calculation of the kinetic parameters must be made from the raw data of the electrochemical measurement and take into account the resistive correction explicitly. Within these limits, the present analysis supports a clear conclusion. Catalyst NiSAs@ACNTF provides the best performance among the series because of the enhanced electrocatalytic capabilities enabled by nickel incorporation.

5. Conclusions

In summary, the presented ZIF-67 derived catalyst sequence demonstrates the kinetic-capacitive-durability relation clearly. The capacitance sequence is ZIF-67 ($7.28\,\mathrm{mF\,cm^{-2}}$) > ZIF-67@DCD ($5.14\,\mathrm{mF\,cm^{-2}}$) > NiSAs@ACNTF ($4.89\,\mathrm{mF\,cm^{-2}}$), while the LSV activity sequence puts NiSAs@ACNTF first. This inversion shows that nickel incorporation does not improve water splitting performance of the catalyst through increased electrochemical accessibility. Rather, it enhances the active sites themselves through favorable Ni-based coordination, as well as the electronic coupling of the carbon skeleton. Chronoamperometry confirms that NiSAs@ACNTF retains higher activity throughout the ten-hour observation window. These results point to a rule in designing MOF-derived water splitting catalysts without noble metals: not just the area, but also active sites quality, electroconductive architecture, and longevity must be optimized. The catalyst with the highest capacitance is not always the best catalyst; the catalyst with high performance is the one that utilizes the accessible area.

References

[1] Seh, Z. W., Kibsgaard, J., Dickens, C. F., Chorkendorff, I., Norskov, J. K., & Jaramillo, T. F. (2017). Combining theory and experiment in electrocatalysis: Insights into materials design. *Science*, *355*, eaad4998.

[2] Roger, I., Shipman, M. A., & Symes, M. D. (2017). Earth-abundant catalysts for electrochemical and photoelectrochemical water splitting. *Nature Reviews Chemistry*, *1*, 0003.

[3] Anantharaj, S., Ede, S. R., Sakthikumar, K., Karthick, K., Mishra, S., & Kundu, S. (2016). Recent trends and perspectives in electrochemical water splitting with an emphasis on sulfide, selenide, and phosphide catalysts of Fe, Co, and Ni: A review. *ACS Catalysis*, *6*, 8069–8097.

[4] Li, Y., Wang, H., Xie, L., Liang, Y., Hong, G., & Dai, H. (2011). MoS_2 nanoparticles grown on graphene: An advanced catalyst for the hydrogen evolution reaction. *Journal of the American Chemical Society*, *133*, 7296–7299.

[5] Zhuang, T., Jia, H., Cao, X., Cheng, Y., Wang, L., Liu, S., & Wang, P. (2021). Non-noble metal electrocatalysts for the hydrogen evolution reaction in water electrolysis. *Electrochemical Energy Reviews*, *4*, 1–36.

[6] Wang, M., Chen, Y., Han, Y., Cui, Y., Ma, C., & Zhang, X. (2020). Efficient tetrafunctional electrocatalyst with synergetic effect of different active sites for multimodel energy conversion and storage. *ACS Applied Materials & Interfaces*, *12*, 23136–23146.

[7] Long, Y., Wang, X., & Zhang, Y. (2025). Evaluation on the potentials of non-nobel metal electrocatalyst in the electrolysis of water. *Analytical Chemistry: A Journal*, *4*, 27–32.

[8] McCrory, C. C. L., Jung, S., Peters, J. C., & Jaramillo, T. F. (2013). Benchmarking heterogeneous electrocatalysts for the oxygen evolution reaction. *Journal of the American Chemical Society*, *135*, 16977–16987.

[9] McCrory, C. C. L., Jung, S., Ferrer, I. M., Chatman, S. M., Peters, J. C., & Jaramillo, T. F. (2015). Benchmarking hydrogen evolving reaction and oxygen evolving reaction electrocatalysts for solar water splitting devices. *Journal of the American Chemical Society*, *137*, 4347–4357.

[10] Anantharaj, S. (2022). Dos and don'ts in screening water splitting electrocatalysts. *Energy Advances*, *1*, 705–707.

[11] Conway, B. E. (1999). *Electrochemical supercapacitors: Scientific fundamentals and technological applications*. Kluwer Academic/Plenum Publishers.

[12] Trasatti, S., & Petrii, O. A. (1991). Real surface area measurements in electrochemistry. *Pure and Applied Chemistry*, *63*, 711–734.

[13] Bard, A. J., & Faulkner, L. R. (2001). *Electrochemical methods: Fundamentals and applications* (2nd ed.). Wiley.

[14] Gong, M., & Dai, H. (2015). A mini review of NiFe-based materials as highly active oxygen evolution reaction electrocatalysts. *Nano Research*, *8*, 23–39.

[15] Zhang, B., Zheng, X., Voznyy, O., Comin, R., Bajdich, M., Garcia-Melchor, M., Han, L., Xu, J., Liu, M., Zheng, L., Garcia de Arquer, F. P., Dinh, C. T., Fan, F., Yuan, M., Yassitepe, E., Chen, N., Regier, T., Liu, P., Li, Y., De Luna, P., Janmohamed, A., Xin, H. L., Yang, H., Vojvodic, A., & Sargent, E. H. (2016). Homogeneously dispersed multimetal oxygen-evolving catalysts. *Science*, *352*, 333–337.